

RADIO MONITORING OF THE TIDAL DISRUPTION EVENT SWIFT J164449.3+573451. II. THE RELATIVISTIC JET SHUTS OFF AND A TRANSITION TO FORWARD SHOCK X-RAY/RADIO EMISSION

B. A. ZAUDERER¹, E. BERGER¹, R. MARGUTTI¹, G. G. POOLEY², R. SARI³, A. M. SODERBERG¹, A. BRUNTHALER⁴, AND
M. F. BIETENHOLZ^{6,7}

Draft version July 18, 2018

ABSTRACT

We present continued multi-frequency radio observations of the relativistic tidal disruption event Swift J164449.3+573451 (Sw 1644+57) extending to $\delta t \approx 600$ d. The data were obtained with the JVLA and AMI Large Array as part of our on-going study of the jet energetics and the density structure of the parsec-scale environment around the disrupting supermassive black hole (SMBH). We combine these data with public *Swift*/XRT and *Chandra* X-ray observations over the same time-frame to show that the jet has undergone a dramatic transition starting at ≈ 500 d, with a sharp decline in the X-ray flux by about a factor of 170 on a timescale of $\delta t/t \lesssim 0.2$ (and by a factor of 15 in $\delta t/t \approx 0.05$). The rapid decline rules out a forward shock origin (direct or reprocessing) for the X-ray emission at $\lesssim 500$ d, and instead points to internal dissipation in the inner jet. On the other hand, our radio data uniquely demonstrate that the low X-ray flux measured by *Chandra* at ≈ 610 d is consistent with emission from the forward shock. Furthermore, the *Chandra* data are inconsistent with thermal emission from the accretion disk itself since the expected temperature of $\sim 30-60$ eV and inner radius of $\sim 2-10R_s$ cannot accommodate the observed flux level or the detected emission at $\gtrsim 1$ keV. We associate the rapid decline with a turn off of the relativistic jet when the mass accretion rate dropped below $\sim \dot{M}_{\text{Edd}} \approx 0.006 M_\odot \text{ yr}^{-1}$ (for a $3 \times 10^6 M_\odot$ black hole and order unity efficiency) indicating that the peak accretion rate was about $330 \dot{M}_{\text{Edd}}$, and the total accreted mass by $\delta t \approx 500$ d is about $0.15 M_\odot$. From the radio data we further find significant flattening in the integrated energy of the forward shock at $\delta t \gtrsim 250$ d with $E_{j,\text{iso}} \approx 2 \times 10^{54}$ erg ($E_j \approx 10^{52}$ erg for a jet opening angle, $\theta_j = 0.1$) following a rise by about a factor of 15 at $\approx 30-250$ d. Projecting forward, we predict that the emission in the radio and X-ray bands will evolve in tandem with similar decline rates.

Subject headings:

1. INTRODUCTION

The unusual γ -ray/X-ray transient Sw 1644+57 has been broadly interpreted as the first example of a tidal disruption event (TDE) powering a relativistic jet (e.g., Bloom et al. 2011; Burrows et al. 2011; Levan et al. 2011; Zauderer et al. 2011). As such, Sw 1644+57 provides unique insight into the formation (and potentially termination) of relativistic jets in supermassive black holes, a process that is not observed in active galactic nuclei due to long lifetimes of $\gtrsim 10^7$ yr. One of the primary observations supporting the TDE relativistic jet scenario in Sw 1644+57 is the long-term evolution of the X-ray light curve, roughly following a $t^{-5/3}$ power law decline (Burrows et al. 2011) as expected for the fallback rate of tidally disrupted material (e.g., Rees 1988). In addition, the mean X-ray luminosity at early time, $L_{X,\text{iso}} \approx 10^{47}$ erg s⁻¹ (flaring to $\approx 3 \times 10^{48}$ erg s⁻¹ on a $\sim 10^2$ s timescale; Burrows et al. 2011), exceeded the Eddington limit of a $\sim 10^6-10^7 M_\odot$ black hole by about 2–3 orders of magnitude, supporting the presence of a collimated relativistic

outflow. Independently, our discovery of bright radio synchrotron emission from Sw 1644+57 established the presence of a relativistic outflow with a Lorentz factor of $\Gamma \sim \text{few}$, launched at the same time as the onset of γ -ray emission (Zauderer et al. 2011; Berger et al. 2012). The basic picture, therefore, is of X-ray emission likely from internal dissipation in the inner part of the jet (at $r \sim 10^{15}-10^{16}$ cm) and radio emission from the expanding forward shock (at $r \sim 10^{18}-10^{19}$ cm).

While the formation of relativistic jets was not predicted in TDE models, a super-Eddington accretion phase was expected (e.g., Evans & Kochanek 1989; Ulmer 1999; Strubbe & Quataert 2009) and the potential for jets was discussed (Giannios & Metzger 2011). The latter paper considered two distinct possibilities for jet formation, during the super-Eddington phase, or at a later time when the accretion rate drops below a few percent of the Eddington rate (motivated by observations of steady jets in X-ray binaries). The rapid formation of the relativistic jet in Sw 1644+57 points to the former scenario. The peak mass accretion rate and duration of the super-Eddington phase are expected to depend on the mass of the black hole, with $\dot{M}_p \approx 1.4 M_\odot \text{ yr}^{-1}$ and $\tau_{\text{SE}} \approx 1.5$ yr for a $3 \times 10^6 M_\odot$ black hole (e.g., Evans & Kochanek 1989; De Colle et al. 2012), the inferred mass of the disrupting supermassive black hole in Sw 1644+57 (Bloom et al. 2011; Burrows et al. 2011; Levan et al. 2011; Zauderer et al. 2011). Although it is unclear what, if anything, happens to a TDE jet when the accretion declines below the Eddington limit, an analogy with X-ray binaries indicates that relativistic jet ejections will likely be restricted to the super-Eddington

¹ Harvard-Smithsonian Center for Astrophysics, 60 Garden Street, Cambridge, MA 02138

² Mullard Radio Observatory, Cavendish Laboratory, Cambridge, CB3 0HE UK

³ Racah Institute of Physics, The Hebrew University, 91904 Jerusalem, Israel

⁴ Max-Planck-Institut für Radioastronomie, Auf dem Hügel 69, 53121 Bonn, Germany

⁶ Department of Physics and Astronomy, York University, Toronto, Ontario, Canada

⁷ Hartebeesthoek Radio Astronomy Observatory, PO Box 443, Krugersdorp, 1740 South Africa

phase (e.g., Fender et al. 1999; De Colle et al. 2012).

To take advantage of this unique opportunity to study the birth and evolution of a relativistic jet from a supermassive black hole, and to track the jet properties of a TDE, we have been carrying out a long-term monitoring campaign of the radio emission from Sw 1644+57, in conjunction with X-ray data (Zauderer et al. 2011; Berger et al. 2012). Here we present new radio observations that extend to $\delta t \approx 600$ d, and use these data to determine the continued evolution of the integrated forward shock energy. We combine these measurements with public *Swift*/XRT and *Chandra* observations over the same timescale to show that the relativistic jet has shut off at $\delta t \approx 500$ d, marked by a steep decline in the X-ray luminosity (Sbarufatti et al. 2012; Levan & Tanvir 2012). The radio data allow us to uniquely determine that the X-ray flux measured in the *Chandra* data is consistent with emission from the forward shock; a model of thermal emission from the accretion disk can be ruled out by the flux and spectrum of the X-ray emission. Associating the rapid decline with the timescale at which $\dot{M} \approx \dot{M}_{\text{Edd}}$, we infer the peak mass accretion rate and the total accreted mass at $\delta t \lesssim 500$ d.

2. RADIO OBSERVATIONS

Previous radio observations of Sw 1644+57 extending to $\delta t \approx 26$ d were presented in Zauderer et al. (2011), while data extending to $\delta t \approx 216$ d were presented in Berger et al. (2012); hereafter, Paper I. Here we report new observations extending to $\delta t \approx 600$ d. All times are measured relative to a γ -ray onset date of 2011 March 25.5 UT. Throughout the paper we use the standard cosmological constants with $H_0 = 70$ km s $^{-1}$ Mpc $^{-1}$, $\Omega_m = 0.27$ and $\Omega_\Lambda = 0.73$.

We observed Sw 1644+57 with the Karl G. Jansky Very Large Array (JVLA⁷) using the Wideband Interferometric Digital Architecture (WIDAR; Perley et al. 2011) correlator to obtain up to 2 GHz of bandwidth at several frequencies. At all frequencies we used 3C286 for bandpass and flux calibration, while phase calibration was performed using J1634+6245 at 1.8 GHz and J1638+5720 at all other frequencies. We reduced and imaged the data with the Astronomical Image Processing System (AIPS; Greisen 2003) software package. The observations are summarized in Table 1.

We also observed Sw 1644+57 with the AMI Large Array (AMI-LA) at 15.4 GHz with a bandwidth of 3.75 GHz using J1638+5720 for phase calibration and 3C48 and 3C286 for flux calibration. The AMI-LA observations are summarized in Table 1.

3. X-RAY OBSERVATIONS

Chandra/ACIS-S observations of Sw 1644+57 (PI: Tanvir; Levan & Tanvir 2012) started on 2012 November 26.42 UT ($\delta t \approx 610$ d), with a total exposure time of 24.7 ks. We analyzed the public data with the CIAO software package (v4.4), using the calibration database CALDB (v4.5.3) and standard ACIS data filtering. Using *wavedetect* we detect Sw 1644+57 at a significance level of 2.8σ with a count rate of $(2.0 \pm 0.9) \times 10^{-4}$ count s $^{-1}$ (0.5–8 keV; 1.5'' radius aperture). We note that emission is detected with a roughly flat distribution in counts s $^{-1}$ keV $^{-1}$ at ≈ 1 –3.5 keV (Figure 1).

To convert the observed count rate to a flux we note that starting at $\delta t \approx 23$ d the X-ray emission from Sw 1644+57

undergoes spectral hardening⁸, with the photon index evolving to $\Gamma \approx 1.3$ at $\delta t \gtrsim 230$ d. We therefore use an absorbed power law spectrum with an index of $\Gamma = 1.3$, intrinsic absorption of $N_{\text{H,int}} = 1.4 \times 10^{22}$ cm $^{-2}$, and Galactic absorption of $N_{\text{H,MW}} \approx 1.7 \times 10^{20}$ cm $^{-2}$ (Kalberla et al. 2005). With this model, the unabsorbed flux is $(5.8 \pm 2.0) \times 10^{-15}$ erg s $^{-1}$ cm $^{-2}$ (0.3–10 keV). For a power law model⁹ with $\Gamma = 2.2$ the resulting flux is only $\approx 5\%$ lower. Finally, a multi-temperature accretion disk blackbody model (*diskbb* in *xspec*) can also fit the data, with a resulting temperature at the inner disk radius of $kT \approx 1$ keV; thermal disk models with a temperature appropriate to a $\sim 10^6$ – 10^7 M $_{\odot}$ supermassive black hole ($kT \lesssim 60$ eV) cannot reproduce the *Chandra* data (Figure 1) and furthermore require an inconsistent radius (see §5).

4. MODELING OF THE RADIO EMISSION

We model the radio emission from Sw 1644+57 following the approach detailed in Paper I, which is based on the afterglow formulation of Metzger et al. (2012) and Granot & Sari (2002). For details of the model we refer the reader to these papers. For the purpose of estimating the X-ray emission from the forward shock we also include in the analysis here the effects of the synchrotron cooling frequency, given by (Granot & Sari 2002):

$$\nu_c = 2.5 \times 10^{14} \epsilon_B^{-3/2} L_{j,\text{iso},48}^{0.5} t_{j,6}^{-1} n_{18}^{-2} \left(\frac{t}{t_j} \right)^{0.5} \text{ Hz}, \quad (1)$$

where ϵ_B is the fraction of post-shock energy in the magnetic fields, $L_{j,\text{iso}}$ is the kinetic luminosity of the outflow, t_j is the timescale over which $L_{j,\text{iso}}$ is assumed to be constant (followed by $L_{j,\text{iso}} \propto t^{-5/3}$ at $t \geq t_j$), n_{18} is the circumnuclear density (n_{CNM}) at a fiducial radius of $r = 10^{18}$ cm, and we use the notation $X \equiv 10^X X_{\text{y}}$. We further assume¹⁰ that $\epsilon_B = 0.01$ and $p = 2.45$.

As in Paper I, we independently model each broad-band radio spectral energy distribution (SED) to extract the temporal evolution of the synchrotron parameters, and in turn the evolution of $L_{j,\text{iso}}$, the emission radius, the jet Lorentz factor (Γ_j), and the radial density profile. The individual SED fits are shown in Figure 2 and the relevant extracted parameters are listed in Table 2. In Figure 3 we plot the light curves at frequencies of 1.8–43 GHz, extending to ≈ 600 d. Finally, in Figure 4 we plot the X-ray data from *Swift*/XRT¹¹ and *Chandra* along with the predicted forward shock emission in the X-ray band based on the radio SED modeling.

5. THE RELATIVISTIC JET SHUTS OFF

The X-ray light curve at $\delta t \approx 15$ –500 d follows a power law decline, with the expected $F_X \propto t^{-5/3}$ (Figure 4; Burrows et al. 2011; Paper I). However, beyond this point the X-ray flux rapidly declines by a factor of about 15 in the span of only 25 days, followed by an additional decline of about a factor of 11 in the subsequent 95 days (see also Sbarufatti et al.

⁸ http://www.swift.ac.uk/burst_analyser/00450158

⁹ This model is appropriate for forward shock emission with $\nu_c < \nu_X$ and $p = 2.45$; see §5.

¹⁰ Note that in Paper I we assumed $\epsilon_B = 0.1$ and $p = 2.5$, which lead to an overall difference in scaling compared to the results here that can be determined from the equations in Paper I. However, the temporal and radial evolution of the kinetic energy and radial density profile presented in Paper I remain unchanged.

¹¹ http://www.swift.ac.uk/xrt_curves/00450158

⁷ The JVLA is operated by the National Radio Astronomy Observatory, a facility of the National Science Foundation operated under cooperative agreement by Associated Universities, Inc. The observations presented here were obtained as part of programs 11A-266 and 12A-280.

2012; Levan & Tanvir 2012). While the X-ray light curve exhibits order of magnitude variability in the first few days, followed by milder variability at later time, a decline by a factor of ≈ 170 in a narrow span of $\delta t/t \lesssim 0.2$ (and by a factor of 15 in $\delta t/t \approx 0.05$) is unprecedented and points to a fundamental change in the nature of the emission. In particular, we conclude that the mechanism powering the X-ray emission at $\delta t \lesssim 500$ d has ceased to operate. The absence of a similar rapid decline in the radio band supports earlier conclusions that the radio and X-ray emission arise from distinct physical components (Bloom et al. 2011; Zauderer et al. 2011; Metzger et al. 2012).

In addition, the rapid decline rules out models in which the X-ray emission at $\delta t \lesssim 500$ d is due to the forward shock or to reprocessing of radiation by the forward shock, since processes at the forward shock are expected to occur on a timescale comparable to the duration of the event, $\delta t/t \approx 1$. Thus, given the rapid decline we conclude that the early X-ray emission originated at a smaller radius than the forward shock, presumably from internal dissipation in the inner part of the relativistic outflow (at $r \sim \text{few} \times 10^{15}$ cm; e.g., De Colle et al. 2012). On the other hand, the low X-ray flux following the steep decline, as measured in the *Chandra* observation, is fully consistent with emission from the forward shock at $r \approx 8 \times 10^{18}$ cm (Figure 4 and Table 2), the same component powering the long-term radio emission.

An alternative explanation for the low X-ray flux at $\delta t \approx 610$ d is thermal emission from the accretion disk itself. In this scenario, for a $3 \times 10^6 M_\odot$ black hole the effective temperature is $kT \approx 25$ eV for an inner radius at the tidal disruption radius, $R_t \approx 12R_s \approx 1.1 \times 10^{13}$ cm (e.g., Ulmer 1999); here R_s is the Schwarzschild radius. The resulting spectral energy distribution severely under-predicts the observed X-ray flux density, and moreover cannot accommodate the X-ray spectrum at $\gtrsim 1$ keV due to the expected steep Wien spectrum. Even a model with a temperature of $kT \approx 60$ eV (corresponding to an inner disk radius of only $2R_s$) cannot accommodate the detected X-ray emission at $\gtrsim 1$ keV (Figure 1). In particular, for this model to even fit the flux normalization of the *Chandra* data at $\lesssim 1$ keV requires an inconsistent inner disk radius of about $40R_s$. A thermal model only fits the data for a high temperature of $kT \approx 1$ keV, but this is not expected for a supermassive black hole. We therefore conclude that forward shock emission is the most natural explanation for the late-time X-ray flux.

While the nature of relativistic jet generation in TDEs is not fully understood, an analogy with X-ray binaries suggests that a powerful jet can be supported as long as the disk is geometrically thick, with an accretion rate of $\dot{M} \gtrsim \dot{M}_{\text{Edd}}$. De Colle et al. (2012) recently presented simulations of the tidal disruption of a $1 M_\odot$ star and showed that for a $3 \times 10^6 M_\odot$ black hole, the peak mass accretion rate is about $240\dot{M}_{\text{Edd}}$ (for order unity efficiency), while $\dot{M} \approx \dot{M}_{\text{Edd}}$ at $\delta t \approx 1.5$ yr. This timescale is remarkably similar to the time of rapid X-ray decline for Sw 1644+57, about 370 d in the rest-frame. Associating this timescale with an accretion rate of about \dot{M}_{Edd} , we find that the beaming-corrected *Chandra* X-ray luminosity of $L_X \approx 2 \times 10^{42}$ erg s $^{-1}$ (for $\theta_j = 0.1$) is about $0.01 L_{\text{Edd}}$ for a $3 \times 10^6 M_\odot$ black hole. However, the resulting low efficiency is not surprising given the hard power index of $\Gamma \approx 1.3$ at $\lesssim 500$ d, which suggests that the bulk of the energy is radiated above the XRT band.

With the inference that $\dot{M}(\delta t = 500 \text{ d}) \approx \dot{M}_{\text{Edd}} \approx 0.006$

$M_\odot \text{ yr}^{-1}$ we can also determine the total accreted mass. Using a simple model with $\dot{M}(t) = \dot{M}_p$ at $\delta t \lesssim 15$ d and $\dot{M}(t) = \dot{M}_p (t/t_j)^{-5/3}$ at $\delta t \gtrsim 15$ d, motivated by the X-ray light curve (Burrows et al. 2011; De Colle et al. 2012; Metzger et al. 2012), we find $\dot{M}_p \approx 350\dot{M}_{\text{Edd}}$, in good agreement with the predictions of De Colle et al. (2012) for a $3 \times 10^6 M_\odot$ black hole. Integrating the mass accretion rate to $\delta t \approx 370$ d in the rest-frame, we find a total accreted mass of $\approx 0.15 M_\odot$. This result is consistent with the disruption of a $\lesssim 1 M_\odot$ star.

In addition to the rapid decline in X-ray emission, which marks the jet turning off, we also find a change in behavior in the integrated energy of the forward shock. Following an increase in $E_{j,\text{iso}}$ by about a factor of 15 at $\delta t \approx 30$ –250 d, our measurements at $\delta t \approx 250$ –600 d point to a mild rise or a plateau at a level of $E_{j,\text{iso}} \approx 2 \times 10^{54}$ erg (Figure 5). For an assumed jet opening angle of $\theta_j \sim 0.1$, this corresponds to a beaming-corrected kinetic energy of $E_K \approx 10^{52}$ erg. The flattening in the temporal evolution of $E_{j,\text{iso}}$ is unlikely to be related to the cessation of jet activity since it begins at an earlier phase. Instead, it is more likely related to the velocity profile of the ejecta, as discussed in Paper I, or to a delayed response of the forward shock to the drop in mass accretion rate below the peak rate (De Colle et al. 2012). As a result, we expect that the turn off of the relativistic jet will have only a mild impact on the forward shock energy, on a timescale of $\delta t \approx 10^3$ d.

6. CONCLUSIONS

We present a joint analysis of radio and X-ray observations of Sw 1644+57 extending to $\delta t \approx 600$ d. From the multi-frequency radio data we determine the integrated energy of the forward shock as a function of time and find that following an increase in $E_{j,\text{iso}}$ by about a factor of 15 at $\delta t \approx 30$ –250 days, measurements to $\delta t \approx 600$ d reveal a mild rise or plateau with $E_{j,\text{iso}} \approx 2 \times 10^{54}$ erg. X-ray observations with *Swift*/XRT and *Chandra* reveal a dramatic change in the light curve evolution, with a sharp decline by about a factor of 170 at $\delta t \gtrsim 500$ –610 d following a steady $t^{-5/3}$ decline at $\delta t \approx 15$ –500 d. Using the radio data, we conclude that the low X-ray flux measured by *Chandra* is consistent with emission from the forward shock. The alternative explanation of thermal disk emission is ruled out by the X-ray flux and spectrum, which instead require a temperature of $kT \approx 1$ keV, compared to an expected value of $\lesssim 60$ eV for a supermassive black hole accretion disk.

The rapid decline suggests that the relativistic jet has turned off, most likely as a result of a decline in the mass accretion rate below $\sim \dot{M}_{\text{Edd}}$. With this interpretation, the overall accreted mass by $\delta t \approx 500$ d is $\approx 0.15 M_\odot \text{ yr}^{-1}$, consistent with the disruption of a solar mass star. Moreover, the rapid decline, with $\delta t/t \lesssim 0.2$, indicates that the X-ray emission at $\delta t \lesssim 500$ d did not originate from the forward shock or from radiation reprocessed by the forward shock. Instead it was likely due to internal dissipation in the inner part of the jet.

Projecting forward, we expect that the X-ray flux evolution will track the decline rate in the optically-thin high-frequency radio bands with a potential dispersion of about ± 0.25 due to the response of the synchrotron cooling frequency to variations in the radial density profile. Additional *Chandra* observations in the coming year will test this prediction.

We thank Ramesh Narayan and Ryan Chornock for de-

tailed and helpful discussions. E. B. acknowledges support from the National Science Foundation through Grant AST-1107973. A. M. S. acknowledges support from the David and Lucile Packard Foundation Fellowship for Science and Engineering. A. B. was supported by a Marie Curie Outgoing International Fellowship (FP7) of the European Union (project

number 275596). The AMI arrays are supported by the University of Cambridge and the STFC. This work made use of data supplied by the UK Swift Science Data Centre at the University of Leicester.

REFERENCES

- Berger, E., Zauderer, A., Pooley, G. G., Soderberg, A. M., Sari, R., Brunthaler, A., & Bietenholz, M. F. 2012, *ApJ*, 748, 36
 Bloom, J. S., et al. 2011, *Science*, 333, 203
 Burrows, D. N., et al. 2011, *Nature*, 476, 421
 De Colle, F., Guillochon, J., Naiman, J., & Ramirez-Ruiz, E. 2012, *ApJ*, 760, 103
 Evans, C. R., & Kochanek, C. S. 1989, *ApJ*, 346, L13
 Fender, R., et al. 1999, *ApJ*, 519, L165
 Giannios, D., & Metzger, B. D. 2011, *MNRAS*, 416, 2102
 Granot, J., & Sari, R. 2002, *ApJ*, 568, 820
 Greisen, E. W. 2003, *Information Handling in Astronomy - Historical Vistas*, 285, 109
 Kalberla, P. M. W., Burton, W. B., Hartmann, D., Arnal, E. M., Bajaja, E., Morras, R., & Pöppel, W. G. L. 2005, *A&A*, 440, 775
 Levan, A. J., & Tanvir, N. 2012, *The Astronomer's Telegram*, 4610, 1
 Levan, A. J., et al. 2011, *Science*, 333, 199
 Metzger, B. D., Giannios, D., & Mimica, P. 2012, *MNRAS*, 420, 3528
 Perley, R. A., Chandler, C. J., Butler, B. J., & Wrobel, J. M. 2011, *ApJ*, 739, L1
 Rees, M. J. 1988, *Nature*, 333, 523
 Sbarufatti, B., Burrows, D. N., Gehrels, N., & Kennea, J. A. 2012, *The Astronomer's Telegram*, 4398, 1
 Strubbe, L. E., & Quataert, E. 2009, *MNRAS*, 400, 2070
 Ulmer, A. 1999, *ApJ*, 514, 180
 Zauderer, B. A., et al. 2011, *Nature*, 476, 425

TABLE 1
RADIO OBSERVATIONS OF SW 1644+57

δt^a (d)	Facility	Frequency (GHz)	Flux Density (mJy)
244.23	JVLA	1.8	2.29 ± 0.08
271.95	JVLA	1.8	2.02 ± 0.23
383.92	JVLA	1.8	4.37 ± 0.10
452.66	JVLA	1.8	3.77 ± 0.09
581.31	JVLA	1.8	2.88 ± 0.08
245.23	JVLA	4.9	12.17 ± 0.05
302.95	JVLA	4.9	12.05 ± 0.05
383.92	JVLA	4.9	12.24 ± 0.03
453.66	JVLA	4.9	11.12 ± 0.03
582.31	JVLA	4.9	8.90 ± 0.03
245.23	JVLA	6.7	16.75 ± 0.06
302.95	JVLA	6.7	15.30 ± 0.08
383.92	JVLA	6.7	14.40 ± 0.03
453.66	JVLA	6.7	11.76 ± 0.02
582.31	JVLA	6.7	8.18 ± 0.02
243.09	JVLA	8.6	20.76 ± 0.24
394.72	JVLA	8.6	13.84 ± 0.03
460.67	JVLA	8.6	10.89 ± 0.03
582.21	JVLA	8.6	7.14 ± 0.03
240.25	AMI-LA	15.4	22.06 ± 0.52
247.97	AMI-LA	15.4	22.99 ± 1.20
258.65	AMI-LA	15.4	21.70 ± 1.03
267.86	AMI-LA	15.4	20.45 ± 0.77
270.03	AMI-LA	15.4	21.60 ± 0.13
273.90	AMI-LA	15.4	22.11 ± 0.38
275.76	AMI-LA	15.4	18.84 ± 0.59
278.91	AMI-LA	15.4	21.38 ± 0.22
279.86	AMI-LA	15.4	20.62 ± 0.36
282.87	AMI-LA	15.4	20.36 ± 0.08
289.92	AMI-LA	15.4	18.68 ± 0.22
295.62	AMI-LA	15.4	20.04 ± 0.45
302.98	AMI-LA	15.4	17.31 ± 0.21
312.79	AMI-LA	15.4	19.21 ± 0.35
327.81	AMI-LA	15.4	15.58 ± 0.14
330.81	AMI-LA	15.4	14.99 ± 0.12
332.80	AMI-LA	15.4	14.94 ± 0.22
336.81	AMI-LA	15.4	14.10 ± 0.22
339.73	AMI-LA	15.4	14.55 ± 0.07
344.72	AMI-LA	15.4	12.53 ± 1.85
347.79	AMI-LA	15.4	13.39 ± 0.07
357.53	AMI-LA	15.4	12.75 ± 1.01
364.66	AMI-LA	15.4	12.66 ± 0.24
367.72	AMI-LA	15.4	12.06 ± 0.05
371.68	AMI-LA	15.4	11.57 ± 0.91
373.63	AMI-LA	15.4	11.76 ± 0.11
378.65	AMI-LA	15.4	10.66 ± 0.69
386.44	AMI-LA	15.4	10.62 ± 0.54
394.66	AMI-LA	15.4	9.90 ± 0.11
422.84	AMI-LA	15.4	8.92 ± 0.48
438.64	AMI-LA	15.4	8.85 ± 0.30
444.53	AMI-LA	15.4	8.00 ± 0.36
447.52	AMI-LA	15.4	8.87 ± 0.93
450.46	AMI-LA	15.4	7.57 ± 0.20
457.60	AMI-LA	15.4	8.05 ± 0.20
463.22	AMI-LA	15.4	7.09 ± 0.64
470.48	AMI-LA	15.4	6.90 ± 0.01
477.54	AMI-LA	15.4	6.91 ± 0.55
479.47	AMI-LA	15.4	6.36 ± 0.67
488.49	AMI-LA	15.4	7.01 ± 0.26
492.42	AMI-LA	15.4	6.88 ± 0.37
499.30	AMI-LA	15.4	5.78 ± 0.03
502.36	AMI-LA	15.4	6.54 ± 0.76
513.76	AMI-LA	15.4	6.00 ± 0.77
522.32	AMI-LA	15.4	5.38 ± 0.64
525.29	AMI-LA	15.4	5.47 ± 0.42
528.25	AMI-LA	15.4	5.55 ± 0.20
534.40	AMI-LA	15.4	6.00 ± 0.10
538.26	AMI-LA	15.4	5.36 ± 0.43
550.31	AMI-LA	15.4	5.16 ± 0.35
552.13	AMI-LA	15.4	4.72 ± 0.25
567.36	AMI-LA	15.4	4.46 ± 0.24
592.10	AMI-LA	15.4	4.51 ± 0.27
243.09	JVLA	19.1	21.89 ± 0.10
298.96	JVLA	19.1	15.75 ± 0.06

TABLE 1 — *Continued*

δt^a (d)	Facility	Frequency (GHz)	Flux Density (mJy)
394.72	JVLA	19.1	8.46 ± 0.03
460.67	JVLA	19.1	6.03 ± 0.03
582.21	JVLA	19.1	3.94 ± 0.03
243.09	JVLA	24.4	20.65 ± 0.11
298.96	JVLA	24.4	13.64 ± 0.06
394.72	JVLA	19.1	6.77 ± 0.04
460.67	JVLA	24.4	4.83 ± 0.03
582.21	JVLA	24.4	3.26 ± 0.03
394.72	JVLA	33.4	5.26 ± 0.04
460.67	JVLA	33.4	3.58 ± 0.04
582.21	JVLA	33.4	2.41 ± 0.05
243.09	JVLA	43.6	13.63 ± 0.19
298.96	JVLA	43.6	7.86 ± 0.14

NOTE. — ^a All values of δt are relative to the initial γ -ray detection: 2011 March 25.5 UT.

TABLE 2
RESULTS OF BROAD-BAND SPECTRAL ENERGY DISTRIBUTION FITS

δt (d)	$\log(\nu_a)$ (Hz)	$\log(\nu_m)$ (Hz)	$\log(\nu_c)$ (Hz)	$\log(F_{\nu_a})$ (mJy)	$\log(r_{18})$ (cm)	$\log(\Gamma_{\text{sh}})$	$\log(\Gamma_j)$	$\log(L_{\text{j,iso,48}})$ (erg s ⁻¹)	$\log(n_{18})$ (cm ⁻³)	$\log(n_{\text{CNM}})$ (cm ⁻³)
244	10.04	9.67	13.00	1.99	0.59	0.31	0.35	0.22	1.08	-0.10
301	9.96	9.54	13.09	1.92	0.66	0.30	0.33	0.24	1.07	-0.24
390	9.71	9.38	13.45	1.72	0.79	0.31	0.33	0.25	0.92	-0.66
457	9.62	9.28	13.56	1.64	0.85	0.30	0.33	0.26	0.88	-0.81
582	9.58	9.13	13.58	1.60	0.90	0.28	0.30	0.28	0.90	-0.90

NOTE. — Measured and inferred parameters of the relativistic outflow and environment of Sw 1644+57 from model fits of the individual multi-frequency SEDs shown in Figure 2. The model is described in Paper I, Metzger et al. (2012), and §4.

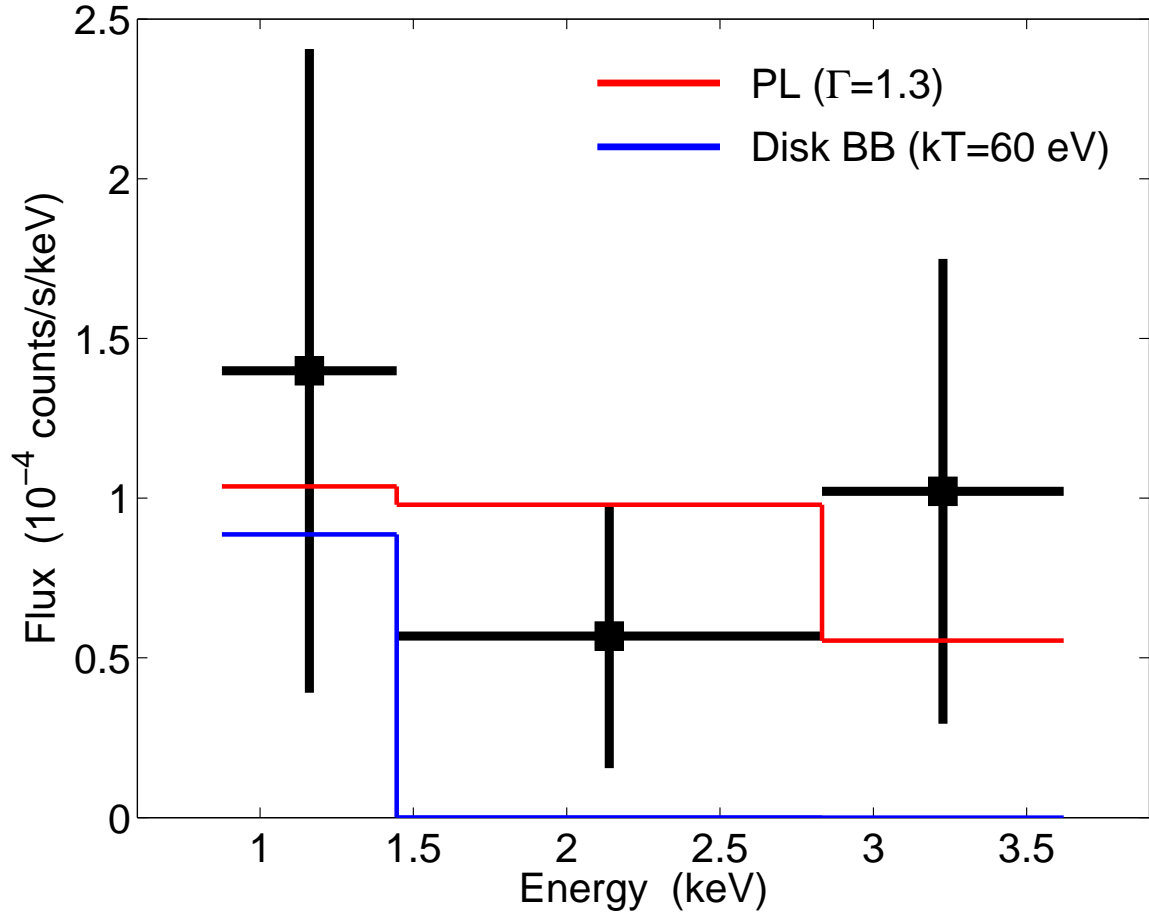


FIG. 1.— Spectrum of the X-ray emission from the *Chandra* observation at $\delta t \approx 610$ d (black points). Also shown are the best fit power law model (red line), and a multi-temperature disk blackbody model with $kT \approx 60$ eV, appropriate for an accretion disk with an inner radius of $2R_s$ around a $3 \times 10^6 M_\odot$ black hole (blue line). The disk model provides a poor fit to the data at $\gtrsim 1$ keV. In addition, to fit the flux at ~ 1 keV this model requires a radius of 3.4×10^{13} cm $\approx 40R_s$, which is inconsistent with the temperature. We therefore conclude that the X-ray emission at late time is not due to the accretion disk.

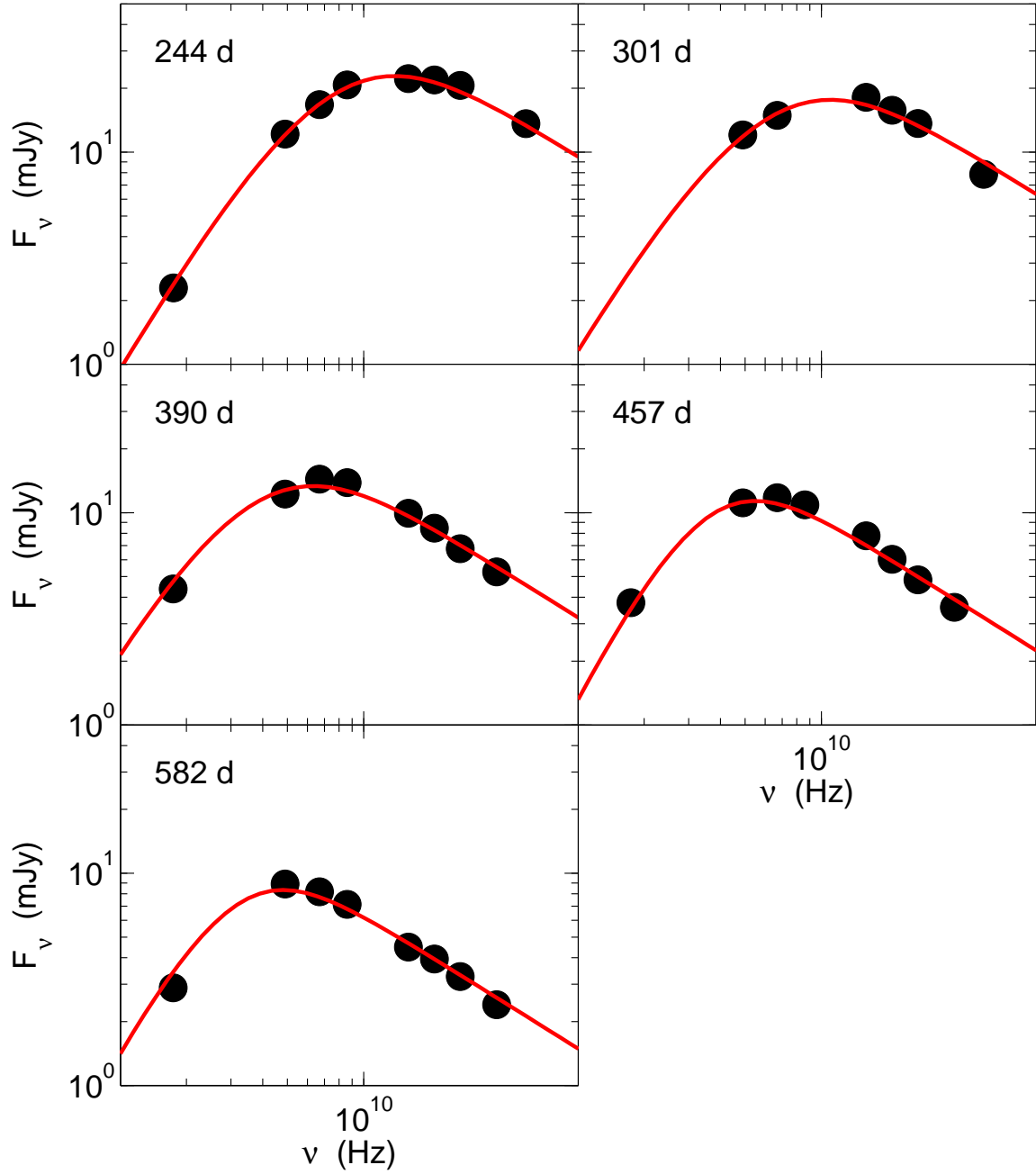


FIG. 2.— Multi-frequency radio spectral energy distributions of Sw 1644+57 at $\delta t \approx 244\text{--}582$ d. The solid lines are fits based on the model described in Paper I, Metzger et al. (2012), and §4. In each epoch we fit for $L_{j,\text{iso}}$ and n_{18} with fixed values of $\epsilon_e = 0.1$, $\epsilon_B = 0.01$, and $p = 2.45$.

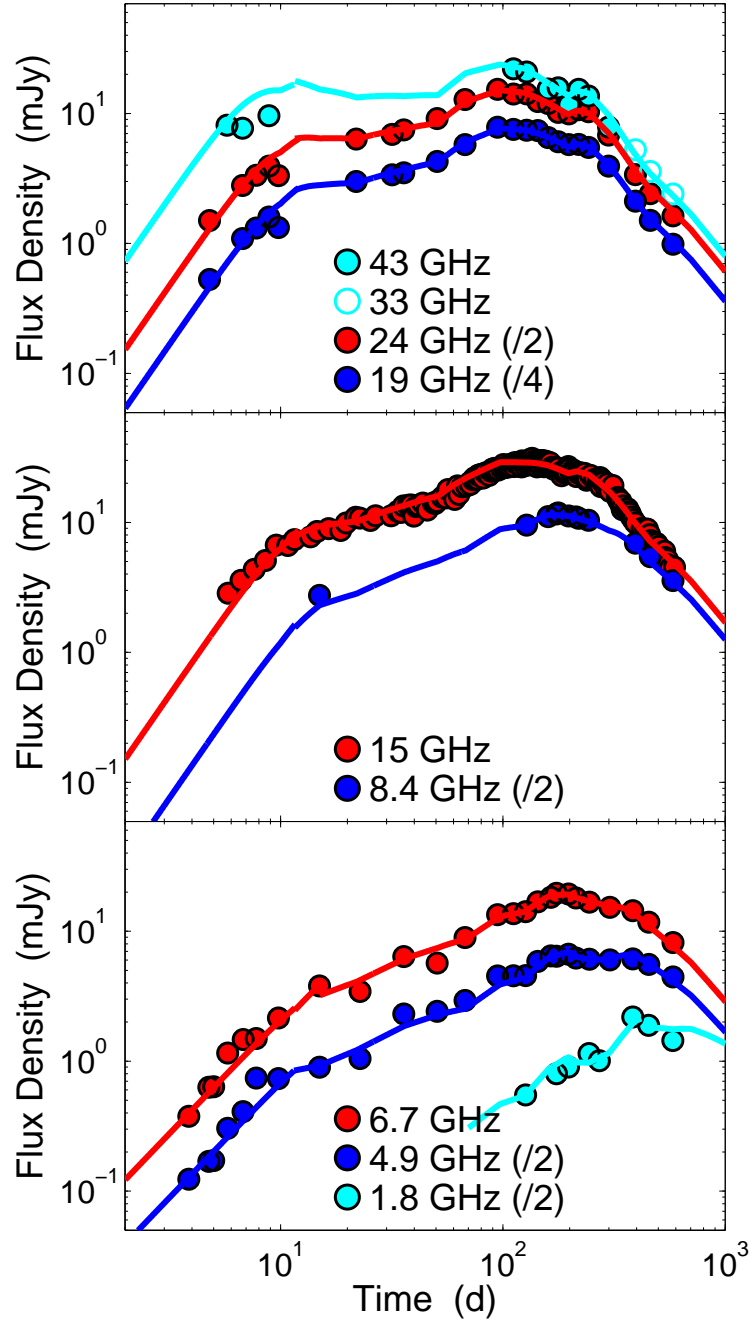


FIG. 3.— Radio light curves of Sw 1644+57 extending to $\delta t \approx 600$ d. The data at $\delta t \approx 5-216$ d were previously presented in Zauderer et al. (2011) and Paper I. The solid lines are models based on independent fits of broad-band SEDs (Figure 2) using the model described in Paper I, Metzger et al. (2012), and §4.

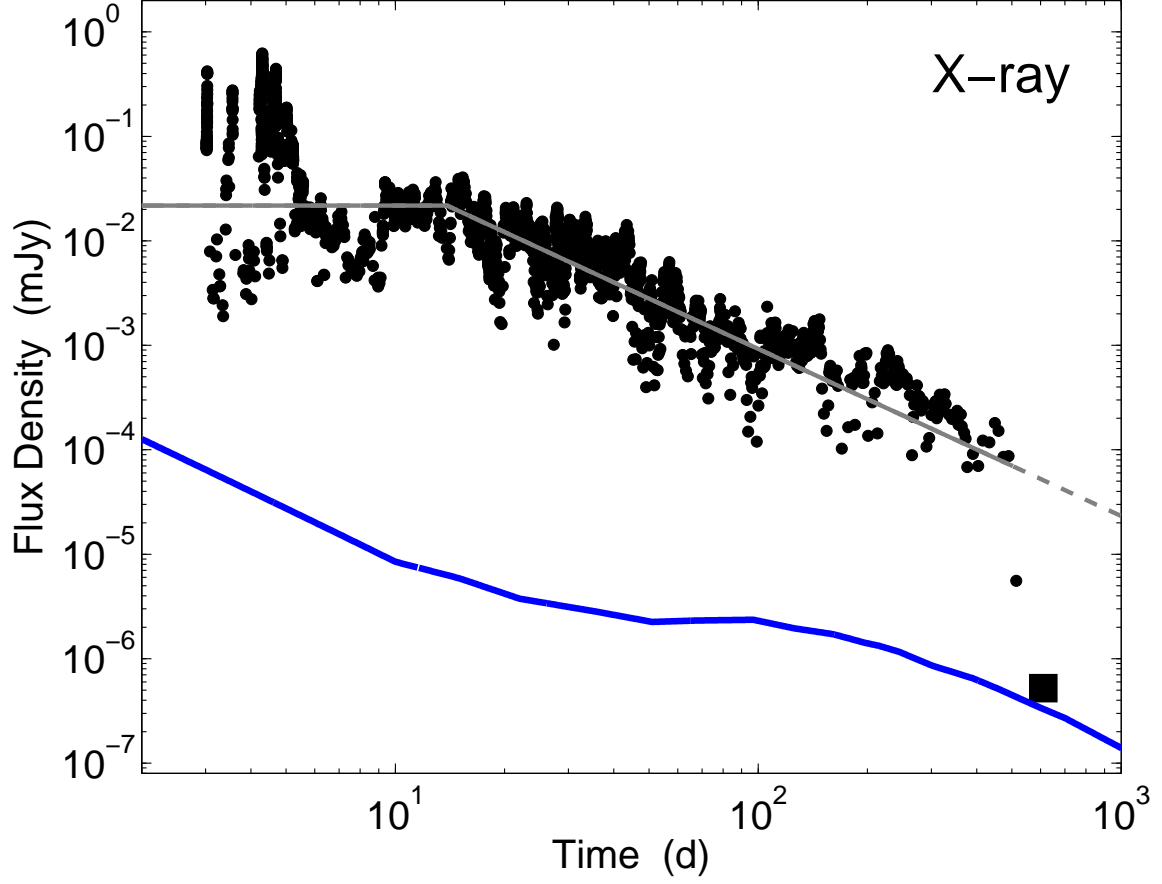


FIG. 4.— X-ray light curve from *Swift*/XRT (circles) and a late-time *Chandra* observation (square). The gray line is a simple model with a constant flux at $\delta t < t_j$ and $F_X \propto t^{-5/3}$ at $\delta t \geq t_j$, with $t_j \approx 15$ d. A rapid decline in the X-ray flux is evident at $\delta t \gtrsim 500$ d. The blue line shows the X-ray emission expected from the forward shock using the synchrotron model described in §4. The model indicates that the flux measured in the *Chandra* observation is consistent with arising from the forward shock.

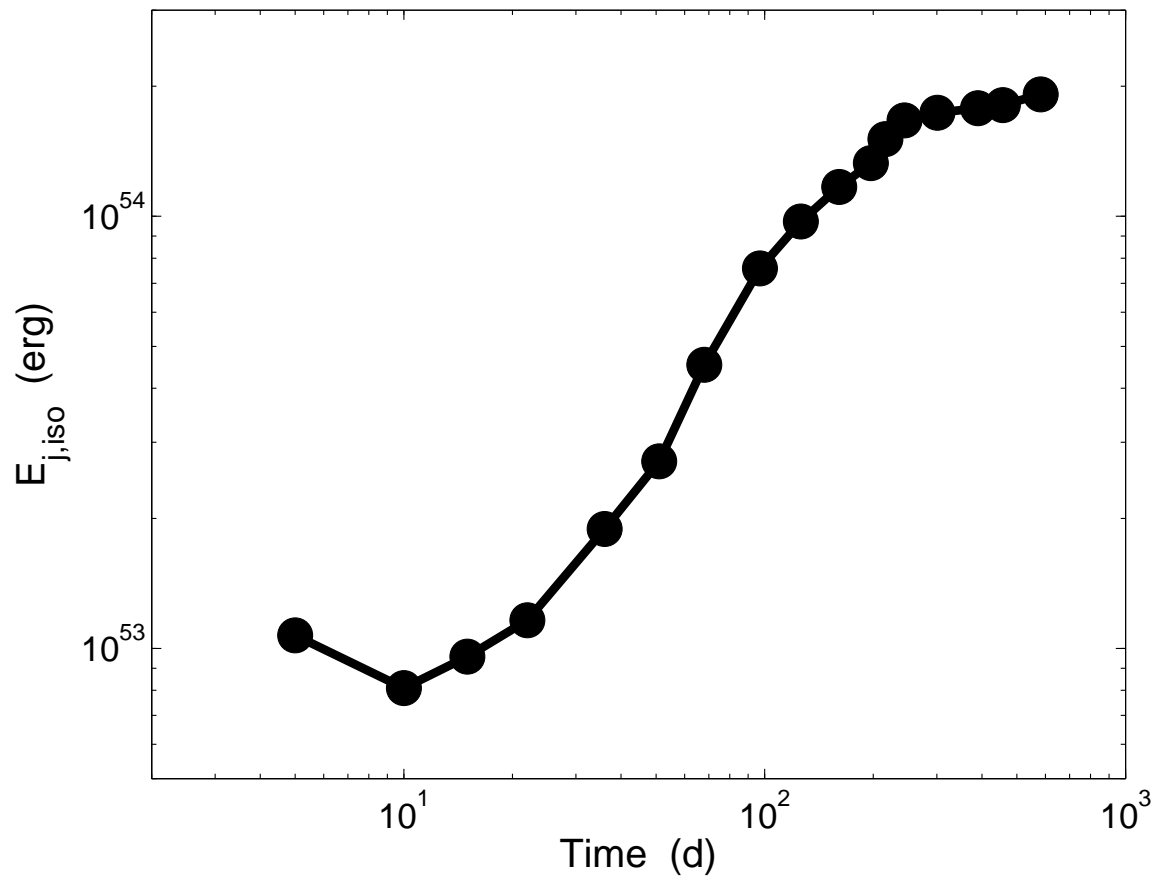


FIG. 5.— Temporal evolution of the isotropic-equivalent integrated kinetic energy ($E_{j,iso} \equiv L_{j,iso} t_j$) based on modeling of the radio emission (Figure 2). The rapid rise at $\delta t \approx 30\text{--}250$ d is followed by a mild rise or plateau to a value of $E_{j,iso} \approx 2 \times 10^{54}$ erg.